Modelling of non-uniform electrical potential barriers for metal surfaces with chemisorbed oxygen

1997 J. Phys.: Condens. Matter 9 5823

(http://iopscience.iop.org/0953-8984/9/27/013)

J. Phys.: Condens. Matter **9** (1997) 5823–5836. Printed in the UK PII: S0953-8984(97)77213-8

Modelling of non-uniform electrical potential barriers for metal surfaces with chemisorbed oxygen

Chang Q Sun†§ and Chunli Bai‡

† Department of Physics, Murdoch University, Western Australia 6150, Australia and Gintic Institute, Nanyang Technological University 638075 Singapore

‡ Institute of Chemistry, Chinese Academy of Sciences, 100080 People's Republic of China

Received 16 August 1996, in final form 5 February 1997

Abstract. A modelling approximation regarding the behaviour of electrons on metal surfaces with chemisorbed oxygen is presented. It is suggested that, as consequences of O–metal surface bonding, ionization, polarization and removal of metal atoms cause the non-uniformity in the surface potential barrier (SPB). The inelastic potential is formulated by using a Fermi-type spatial decay and the work function that depends on the occupied density of state. This formulation takes into account that, at energies below the plasma excitation energy, electron excitation dominates and that the electron excitation occurs in the electron-occupied space with any energy greater than the work function. The present modelling method is an improvement in that (i) the elastic potential, the spatial decay and the energy dependence of the inelastic potential are associated with the electron distribution, $\rho(z)$; (ii) all the SPB parameters are functionalized as dependents of the origin of the image plane, z_0, or the boundary of the region occupied by electrons; (iii) the spatial localization and the variation in energy state are taken into account; and (iv) the single-variable parameterized SPB simplifies the very-low-energy electron diffraction calculations and ensures the uniqueness of the solutions. This method allows us to optimize crystal structures by uniquely comparing the shapes of the geometry-dependent $z_0(E)$ curves that exhibit joint features of topography and spectroscopy revealed by STM/STS.

1. Introduction

The potential barrier of a surface (SPB) originates from the charge distribution both in real space and in energy space [1, 2] which is closely linked to the valence states and geometrical arrangement of atoms on the surface [3–5]. For clean metal systems, such as Cu(001) [6–8], W(001) [9] and Ru(110) [10] as well as Ni [11], the SPB has been modelled successfully as a uniform layer of thin-film interference [1, 6, 9, 10] and the inelastic damping as monotonically energy-dependent [11]. Scanning tunnelling microscopy/spectroscopy (STM/S) observations [12–16] have provided evidence that the uniform-SPB approximation [9, 11] for clean metals is complete and correct [6]. For example, STM reveals that ion cores with small protrusions (0.15–0.30 Å) are arranged regularly in the homogeneous background or Fermi sea [12–16] and STS studies of the Cu(110) surface by Chua *et al* [13] confirmed the uniformity of the density of state (DOS) below E_f. Hence the clean metal surfaces can be described as ideal Fermi systems and the uniform-SPB approximation is practical and acceptable. Surfaces with chemisorbed oxygen differ from those of the pure metals in that they possess the unusual feature that

§ E-mail address: cqsun@gintic.gov.sg

0953-8984/97/275823+14$19.50

many properties are 'rather local' [15, 16]. The chemisorption of oxygen results not only in the dislocation of ion cores but also in the alternation of atomic sizes and states [3–5, 13]. More importantly, as consequences of O–metal bonding, the formation of the dipole layer and the removal of missing-row atoms, in some cases, roughen the surface [3–5, 11–18]. These features have been identified with STM/S and other techniques as well. Even at very low exposures to oxygen, the Cu(001) surface is roughened by the protruding domain boundaries, as was discovered recently by Fujita *et al* [19]. The STM scale differences of the systems with chemisorbed oxygen are much higher (0.45–1.2 Å) [12–16, 19] than those of pure metals. The STS profiles from the O–Cu chain region on the O–Cu(110) surface [13] show that there is a general elevation of energy states, which concurs with the results of the effective-medium theory calculations by Nørskov *et al* [16, 20]. In particular, the empty surface state above E_f is occupied and a new DOS is generated below E_f [13]. Patches of protrusions on the O–Pt surfaces give rise to the reduction in the work function (by about 1.2 eV) were detected with photo-electron-emission microscopy by Rotermund *et al* [21]. In calculations of very-low-energy electron diffraction (VLEED) from the O–Cu(001) surface [3, 6], it was found that the spectrum collected at azimuth close to the $\langle 11 \rangle$ direction (perpendicular to the missing row) could not be simulated with the uniform SPB by using the Cu(001)-c(2 × 2)-O [22] the ($\sqrt{2} \times 2\sqrt{2}$)R45°-O [23] structure or their combination. Therefore, it seemed implausible with VLEED to determine both the SPB and the crystal structure simultaneously by dealing with the strongly correlated parameters independently [6]. The atomic-scale localization and the on-site variation of energy states of the systems with chemisorbed oxygen suggest that it is necessary to consider the electron distribution on the surface site by site. The three-dimensional effect, the variation in energy states of the surface and the correlations among the parameters used in calculations constitute the complexity in de-coding VLEED data from the systems with chemisorbed oxygen and these components can never be neglected. Therefore, it is necessary to develop a non-uniform-SPB model for systems with chemisorbed oxygen.

The objective of this work is to show that such a non-uniform-SPB model can be formulated. The modelling was intended to (i) reduce the number of independent variables in the SPB to simplify VLEED optimization and to ensure the uniqueness of solutions; (ii) allow the calculation code to optimize the single-variable $z_0(E)$ automatically to replicate the experimental data; (iii) let the $z_0(E)$ profile vary with the crystal structure to reflect appropriately the interdependence between the atomic geometry and electronic properties; and, eventually, (v) gain deeper insight into the behaviour of electrons on metal surfaces with chemisorbed oxygen.

2. The theoretical model

2.1. The physical foundations

2.1.1. Constraints. Electrons with energy E traversing the surface region can be described as moving in a complex optical potential [2]:

$$V(\boldsymbol{r}, E) = \mathrm{Re}\, V(\boldsymbol{r}) + \mathrm{i}\, \mathrm{Im}\, V(\boldsymbol{r}, E) = \mathrm{Re}\, V(\boldsymbol{r}) + \mathrm{i}\, \mathrm{Im}\, [V(\boldsymbol{r}) V(E)]. \qquad (1)$$

$V(\boldsymbol{r}, E)$ satisfies the following constraints.

(i) The elastic potential, $\mathrm{Re}\, V(\boldsymbol{r})$, satisfies Poission's equation $\nabla^2[\mathrm{Re}\, V(\boldsymbol{r})] = -\rho(\boldsymbol{r})$ [9, 24], and its gradient relates to the intensity of the electric field ε, $\nabla[\mathrm{Re}\, V(\boldsymbol{r})] = -\varepsilon$. If $\rho(\boldsymbol{r}) = 0$, then $\mathrm{Re}\, V(\boldsymbol{r})$ corresponds to a conservation field; that is, the moving electrons will suffer no energy loss and the spatial variation of the inelastic potential

$\mathrm{Im}\,V(\boldsymbol{r}) = 0$. Thus, $\mathrm{Im}\,V(\boldsymbol{r})$ is correlated with $\mathrm{Re}\,V(\boldsymbol{r})$ uniquely through the electron distribution $\rho(\boldsymbol{r})$ as indicated in figure 1.

(ii) The energy dependence of the inelastic potential $\mathrm{Im}\,V(E)$ reflects the effect of all the dissipative processes that are dominated by phonon and single-electron excitation at energies below the plasma excitation energy [1, 2]. The single-electron excitation occurs in the electron-occupied space, described by $\rho(\boldsymbol{r})$, and with any energy E greater than the work function ϕ [1, 2, 6, 9].

(iii) The z directional integrations of $\mathrm{Im}\,V(z, E)$ and $\mathrm{Re}\,V(z)$ correspond to the amplitude loss and the phase change of the electron beams [6, 9]. This constraint provides leeway for the mathematical expressions for $\mathrm{Re}\,V(z)$ and $\mathrm{Im}\,V(z, E)$. Hence, the specific forms of $\mathrm{Im}\,V(z)$, $\mathrm{Im}\,V(E)$ and $\mathrm{Re}\,V(z)$, and therefore the exact values of the strongly correlated parameters, are much less important than are the two integrations in the physics. The independent treatment of the correlations among the SPB parameters leads to infinite numerical solutions that should correspond to reality and be physically meaningful.

(iv) On the other hand, the variation in atomic geometry and the change in electronic states both in real space and in energy space depend on each other insofar as they are consequences of the surface bonding [3–5].

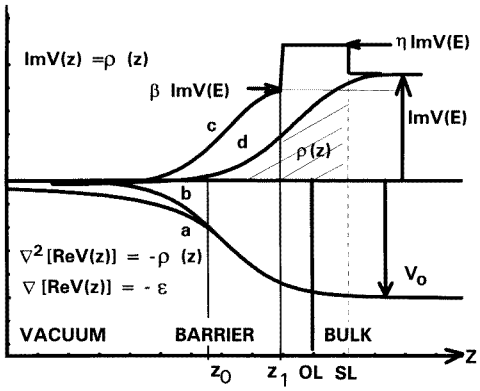

Figure 1. An illustration of the prototype of the non-uniform SPB. Curves (a) and (b) are $\mathrm{Re}\,V(z)$ [8] and the quasi-Fermi z function. Curve (c) is the conventional step–Gaussian decay [6, 7] of the damping, in which β and η are independent parameters used to modulate the intensities in different regions. Curve (d) is the Fermi z function proposed in this work to model the spatial electron distribution, $\rho(z)$. $\mathrm{Im}\,V(z)$ correlates with $\mathrm{Re}\,V(z)$ through $\rho(z)$ as indicated.

2.1.2. Uniform-SPB approaches. The best model of $\mathrm{Re}\,V(z)$ currently in use was formulated by Jones, Jennings and Jepsen [9] in 1984 on the basis that it closely approximated the results of jellium and density functional calculations of the SPB. This model has been used widely for the fitting both of the VLEED fine-structure features and of the inverse-photoemission image states, and has the form [9]

$$\mathrm{Re}\,V(z) = \frac{-V_0}{1+A\exp[-B(z-z_0)]} \qquad z \geqslant z_0 \text{ (a pseudo-Fermi } z \text{ function)}$$
$$= \frac{1-\exp[\lambda(z-z_0)]}{4(z-z_0)} \qquad z < z_0 \text{ (the image potential)} \qquad (2)$$

where A and B are constants given by $B = V_0/A$ and $A = -1 + 4V_0/\lambda$. The z axis is directed into the crystal. V_0 is the muffin-tin inner potential constant of the crystal and z_0 is the origin of the image potential. The degree of saturation is described by the λ parameter.

$\mathrm{Re}\,V(z)$ changes its form at $z = z_0$ from the pseudo-Fermi z function to the $1/(z - z_0)$-dominated classical image potential. It can be readily justified that $\nabla^2[\mathrm{Re}\,V(z_0)] = -\rho(z_0) = 0$. Therefore, the origin of the image plane, z_0, acts as the boundary of the region occupied by surface electrons. If we permit z_0 to vary with the surface coordinates, then $z_0(x, y)$ provides a contour of the spatial electron distribution similar to the STM image. The SPB features are thus characterized by z_0 and this effect allows us to choose z_0 as the character in the subsequent single-variable functionalization of the non-uniform SPB, as will be discussed.

The *energy dependence* of the inelastic damping, $\mathrm{Im}\,V(E)$, for a pure metal was proposed empirically by McRae and Caldwell [11] in 1976 from their VLEED investigations of Ni surfaces. This model also performs well in dealing with other metal surfaces [6–8]. The damping varies with energy monotonically:

$$\mathrm{Im}\,V(E) = \gamma(1 + E/\phi)^{\delta} \qquad (\gamma = -0.26, \delta = 1.7) \tag{3}$$

where ϕ is the work function of the crystal studied.

The *spatial decay* of the inelastic damping, $\mathrm{Im}\,V(z)$, was not known and it was expressed typically with step and Gaussian-type functions [7, 8]:

$$\begin{aligned} \mathrm{Im}\,V(z) &= \beta \exp[-\alpha|z - z_1|] \qquad (z < z_1) \\ &= \eta \qquad\qquad\qquad\qquad (z_1 < z < Z_{SL}) \end{aligned} \tag{4}$$

where β, α, η and z_1 are adjustable parameters to be fixed in calculations. β and η were employed to modify the intensity of damping in various regions. Z_{SL} is the atomic position of the second layer.

It is to be noticed that $\mathrm{Re}\,V(z)$, $\mathrm{Im}\,V(z)$ and $\mathrm{Im}\,V(E)$ (equations (2)–(4)) are independent from one another. In figure 1, curve (a) corresponds to $\mathrm{Re}\,V(z)$ and curve (b) illustrates the pseudo-Fermi z function. Curve (c) is the step–Gaussian-type $\mathrm{Im}\,V(z)$ and curve (d) the Fermi z decay $\rho(z)$ proposed in this work.

2.2. The single-variable functionalized non-uniform SPB

2.2.1. Local density of states and the local work function. Instead of the complex form of $\rho(z)$ derived from the Poission equation (constraint (i)), we may define a Fermi z function, as was used in [4–6], as a form of the spatial decay $\mathrm{Im}\,V(z)$ to model the electron distribution (figure 1, curve (d)):

$$\rho(z) = \frac{V_0}{1 + \exp[-(z - z_1)/\alpha]}. \tag{5}$$

$\rho(z)$, characterized by z_1 and α, is constrained by $\rho(z_0) \approx 0$. The z directional integration of $\rho(z)$ outside the second layer of the lattice is therefore proportional to the occupied local density of states (DOS), $n(x, y)$. The region of integration was determined on the basis that the inelastic damping shall dominate in this region [4].

It is essential to introduce the corresponding concept of the local work function $\phi_L(x, y)$ [25]:

$$\phi_L(x, y) = E_0 - E_f \left(\frac{n(x, y)}{n_0}\right)^{2/3} \tag{6}$$

where $E_0 = 12.04$ eV and $E_f = 7.04$ eV are the vacuum and Fermi levels of a pure Cu surface. For calibration n_0 was given by the data for the Cu(001) surface ($V_0 = 11.56$ eV, $z_1 = z_0 = -2.5$ Bohr radii, $1/\alpha = \lambda = 0.9$) [8]. Different calibrations provide merely off-set shifts of the $\phi_L(x, y)$ value, which were not that serious, as we had expected.

It is worth emphasizing that the work function depends on the electron density and it is independent of the dimensions of whatever sample is being considered [25]. The idea of the local work function ϕ_L was addressed in 1994 by Ertl [26] who considered variations on the scale of patches of unit cells [21] for chemisorption of oxygen. Here it is suggested that the concept can be extrapolated to the atomic scale so that variations occur over the dimensions of a single unit cell. For metal systems with chemisorbed oxygen, the usual concept of ϕ is no longer valid due to the 'strong local' features, as they are widely known [3–5, 12–16]. It is even unlikely that the strongly localized electrons with low mobility move from the site of 'lower' ϕ_L to the site of 'higher' ϕ_L in the described ϕ_L system. Since VLEED integrates over a large area of surface, all the quantities depending on (x, y) become energy-dependent ones. Accordingly, $n(x, y)$ in ϕ_L becomes $n(E)$. $n(E)$ is precisely the occupied DOS that is characterized by $z_0(E)$ bounding the region occupied by electrons. In the current modelling approach, the ϕ_L depending on E is also extended to large surface areas over which VLEED integrates for the DOS.

2.2.2. Parameterization of the non-uniform SPB. Under the constraints (i)–(iii) in section 2.1, we may define an inelastic potential to unite the effect that damping occurs in the electron-occupied space (Fermi z decay) with any energy greater than the work function, which depends on the occupied DOS:

$$\begin{aligned}\operatorname{Im} V(z, E) &= \operatorname{Im} V(z) \operatorname{Im} V(E) \\ &= \gamma\rho(z) \exp[(E - \phi_L)/\delta] \\ &= \frac{\gamma \exp\left(\frac{E-\phi_L(E)}{\delta}\right)}{1 + \exp\left(-\frac{z-z_1(z_0)}{\alpha(z_0)}\right)}\end{aligned} \tag{7.1}$$

where γ and δ are constants depending on the calibration of the measured spectral intensities. $z_1(z_0)$ and the $\alpha(z_0)$ in the Fermi z function characterize the electron distribution. $\rho(z_1)$ should be half of the bulk electron density. In order to reduce numerical efforts and ensure the uniqueness of solutions, it is necessary to define them as functional dependents on z_0. They are simply supposed to be correlated with z_0 through a Gaussian-type function:

$$z_1(z_0) = z_0 \exp\left[-\left(\frac{z_0 - z_{0M}}{\tau_1}\right)^2\right] \tag{7.2}$$

$$\alpha(z_0) = \frac{1}{\lambda(z_0)} \exp\left[-\left(\frac{z_0 - z_{0m}}{\tau_2}\right)^2\right]. \tag{7.3}$$

The constants τ_1 and τ_2 are the semi-widths of the Gaussian functions and were optimized to 0.75 and 1.50 by producing the smallest Δz_0 in the calculation results [4, 5]. z_{0m} was estimated to be -1.75 Bohr radii.

As will be justified in section 4.1, λ (in equation (2)) increases monotonically with the outwards shift of z_0:

$$\lambda(z_0) = \lambda_{0M}\left\{x + (1 - x) \exp\left[-\left(\frac{z_0 - z_{0M}}{\lambda_z}\right)^2\right]\right\} \qquad (x = 0.4732) \tag{8}$$

where the $\lambda_{0M} = 1.275$ is the maximum of λ corresponding to $z_{0M} = -3.425$ Bohr radii and $\lambda_z = 0.8965$. These constants, which may vary with materials examined were obtained by least-square simulation of a $z_0(E)$–$\lambda(E)$ curve that was obtained from point-by-point calculations by keeping other parameters constant [6]. This process is not of immediate concern insofar as it is much less important than the modelling approaches.

Equations (7.2), (7.3) and (8) represent not only correlations among SPB parameters but also hypotheses that, at the dipole site, $z_{1M} \approx z_{0M}$, $\alpha \leqslant \lambda^{-1}$, whereas in the missing-row position, $z_{1m} \ll z_{0m}$ and that $\mathrm{Im}\, V(z)$ is much less saturated than is $\mathrm{Re}\, V(z)$ in the missing-row vacancy. The SPB increases its degree of saturation with the outwards shift of the image plane z_0.

2.2.3. Schematic interpretations of the SPB. Figure 2 shows an interface between the bulk and the vacuum for typical O–metal surfaces to illustrate the coordinate dependences of z_0 and z_1 in the SPB, $\mathrm{Re}\, V(z)$ and $\mathrm{Im}\, V(z)$. This interface can ideally suit the Cu(110)$-(2 \times 1)-$O case crossing the O–Cu chains [3]. The z axis originating from the top layer (OL) is directed into the bulk. The two typical broken curves, at the sites of the dipole and the missing-row vacancy, are $\mathrm{Re}\, V(z)$ of figure 1(a) [9] to illustrate the difference in z_0 and λ from site to site on the surface. That $z_0(x, y)$ is usually higher than $z_1(x, y)$ results from the contribution of the surrounding electrons to the image potential. It is also to be noted that $\rho(z_1) = \frac{1}{2}\rho(z \geqslant z_{SL}) > \rho(z_0) \approx 0$, as defined by the Fermi z function and the correlation between $\mathrm{Re}\, V(z)$ and $\mathrm{Im}\, V(z)$. In the vacant position, the minimum z_{1m} is much lower than z_{0m} because it is assumed that no free electrons flow into the missing-row vacancy. In the dipole position, the maximum $z_{1M} \approx z_{0M}$ is due to the formation of metal dipoles resulting in the shifting outwards and the saturation of electron clouds [14, 15]. Hence, the higher z_0, the higher the degree of saturation of the SPB (equations (7.2), (7.3) and (8)). Consequently, the higher the protrusion in the STM image the higher the local DOS and, as a result, the lower the work function (equation (6)). Apparently, just like the gradient of $\mathrm{Re}\, V(z)$, the intensity of the electric field at the surface should also be site-dependent (see constraint (i) and figure 1). At the dipole site, the electric field is much stronger than that at a clean surface or in the STM depressions. At distances sufficiently far away from the surface, the SPB approaches the conventional uniform type.

2.2.4. The significance and limitations of this work. A new model of a single-variable parameterized non-uniform SPB has been developed for metal surfaces with the chemisorbed oxygen. Instead of being independent, $\mathrm{Re}\, V(z)$ (equation (2)) and the current $\mathrm{Im}\, V(z, E)$ (equation (7.1)) are tied closely together through the surface charge distribution $\rho(z)$, as indicated in figure 1. Except for the inner potential constant V_0, the parameters λ, α and z_1 are functional dependents of z_0. The number of variables of the current model is hence reduced from four to one. This single-variable parameterization allows the calculation code to optimize z_0 automatically to give intensity matching between calculation and measurement at each energy. If the character z_0 remains constant $\mathrm{Re}\, V(z)$ and $\mathrm{Im}\, V(z, E)$ will degrade to the conventional form, namely, a one-dimensional uniform and monotonic energy dependence.

Besides, as will be shown, the $z_0(E)$ profile varies with the atomic position, which satisfies constraint (iv). The connection of the SPB to the crystal geometry reasonably well represents that the crystal structure and the SPB are interdependent insofar as they are consequences of surface bonding [3–5]. It now becomes possible to determine crystal and electronic properties simultaneously with VLEED by analyzing the structure dependent

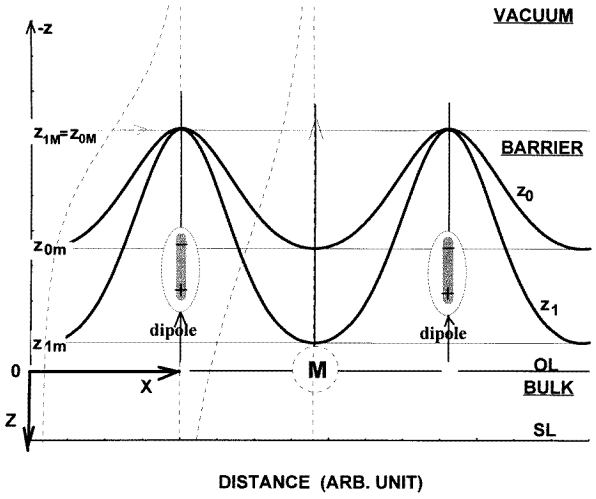

Figure 2. The coordinate (viewed in the x–z plane) dependence of z_0 and z_1 characterizing the three-dimensional SPB. The bulk ($z >$ OL), barrier and vacuum regions are indicated. That z_0 is usually higher than z_1 results from the contribution of the surrounding electrons to the image potential characterized by z_0. At distances sufficiently far away from the surface the SPB approaches uniformity. The broken lines are the $\mathrm{Re}\,V(z)$ corresponding to the locations at the dipole and the missing-row vacancy, showing the difference in degree of saturation.

$z_0(E)$ profile. Therefore, the difficulty (in conventional wisdom) has been overcome completely. On the other hand, the variation of the energy state represented by $z_0(E)$, which is an important aspect of chemisorption studies, can also be probed.

However, processes such as band transition and single excitation adding humps to the monotonic damping [6] (due to a uniform DOS or a constant work function) are not apparent in the present form (equations (7.1)–(7.3)), but one can compensated for these by a z_0-optimizing method based on the premise that the work function depends on the DOS, as demonstrated below.

3. VLEED calculations

The validity of the proposed SPB model was tested by analyzing the high-resolution VLEED (00) beam spectrum from a Cu(001) surface exposed to the equivalent of 300 Langmuir of oxygen. The technique and procedures of data acquisition were described previously by Hitchen *et al* [27]. Attention was paid to the spectrum at 43.5° azimuth which could not be fitted with the uniform-SPB approximation [6]. Calculations were performed with a multi-atom code developed from the package of Van Hove and Tong [28]. Its validity was demonstrated and a full description of the calculation code given in [6].

With respect both to the resolution of a VLEED spectrometer and to the convergence intensity in calculations, the maximum reflectivity (I_{00}/I_0) was calibrated as 10%. The inaccuracy of the calibration can be compensated for by adjusting the constants γ and δ in equation (7.1) [4].

In calculations, we employed the widely accepted missing-row type Cu(001)-($\sqrt{2} \times 2\sqrt{2}$)R45°-O reconstruction model [3, 12, 16, 20, 22, 23, 29]. The complex unit cell and the parameters of the compared structures are illustrated in figure 3 and listed in table 1. The

atomic-shift parameters are the layer spacing, the displacements of the O adsorbate and the Cu atoms (D_{12}, DO_x, DO_z, DCu_x and DCu_z in figure 3). The atomic positions in A were given by a bond geometry that was presented in [3] and used in [4, 5]. This structure was developed using the theories of Keenan *et al* [30], Pauling [31] and Goldschmidt [32] regarding the nature and geometry of oxygen-related bonding. This model (a perspective view was given in [4, 5]) coincides with a recent discovery [33] concerning other O–Cu systems that the two O^{2-} get 'four electrons from three coppers', and represents the reaction

$$\begin{aligned} &4\text{Cu(surface)} + 2\text{Cu(substrate)} + \text{O}_2\text{(adsorbate)} \\ &\qquad \rightarrow 2\text{O}^{2-}\text{(hybrid)} + 2\text{Cu}^{+}\text{(substrate)} + \text{Cu}^{2+}\text{(surface)} \qquad (\text{Cu}_3\text{O}_2 \text{ bonding}) \\ &\qquad +2\text{Cu(buckled dipole)}+\text{Cu(missing-row vacancy)} \qquad \text{(a bonding effect).} \end{aligned} \tag{9}$$

The calculation procedures are as follows. First, referring to the value of z_0 for a clean Cu(001) surface which is in the range from the jellium edge to the atomic radius [6–8], we let the calculation code scan z_0 over -2.5 [8] ± 1.0 Bohr radii, with a step of $\delta z_0 = 0.25$ Bohr radii so as to examine the uniqueness of solutions. The output of the z_0-scanning calculation is the z_0–E contour. This contour plot also assists us in optimizing the constants (such as γ, δ, τ_1 and τ_2) involved in the SPB functions (equations (7.1)–(7.3) and (8)). Then, after all the constants have been fixed, the calculation code automatically optimizes $z_0(E)$ (with a step of $\delta z_0 = 0.0001$–0.25 depending on the value of I_c/I_m) to match the calculated I_c with the measured I_m at each energy. The outcomes of the z_0-optimizing method are eventually the duplication of the measured I_m and the corresponding energy dependence of $z_0(E)$. This method is thus able to compensate for the defect of equation (7.1) in describing the damping due to electron excitation.

Table 1. Crystallographic and microscopic information about the compared models.

Parameter	A [3–5]	B [23]	C [29]	D [20]
D_{12}	1.9343	1.94	2.06	1.94
DCu_x	0.250	0.3	0.1	0.3
DCu_z	−0.1495	−0.1	−0.2	−0.1
DO_x	−0.1876	0.0	0.0	0.0
DO_z	0.1682	−0.2	−0.1	0.0
$-z_{0M}$ (au)	3.373	3.615	3.676	3.623
$-z_{0m}$ (au)	2.386	2.261	2.385	2.223
Δz_0 (Å)	0.522	0.717	0.683	0.741

We need to set up criteria for the optimal $z_0(E)$ profiles. In conventional wisdom, it is expected that $z_0(E)$ approaches a constant. This is valid for pure metal surfaces with homogeneous energy states and small ion-core corrugations [12–14] but it is no longer true for the systems with chemisorbed oxygen. As will be explained, the current $z_0(E)$ should be in any form exhibiting joint features of topography and spectroscopy other than traditional constant or monotonically energy-dependent ones. With respect both to the conventional wisdom and to the feature of the new SPB showing humps due to electron excitation, the criteria for selecting the $z_0(E)$ curves were set as follows: (i) the solution of $z_0(E)$ is finite; (ii) Δz_0 is as small as possible and (iii) the fewest possible extra features appear on the $z_0(E)$ curve.

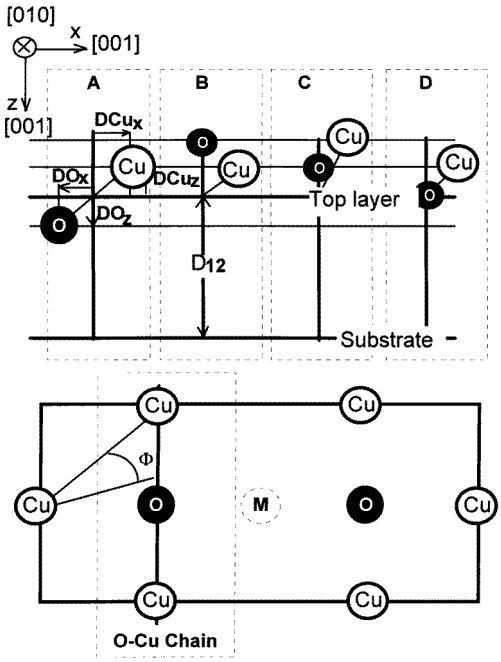

Figure 3. Side and top views (of the bottom unit cell) of the compared crystal structures in the missing-row model. The four different sets (A–D) of atomic dislocations along the O–Cu chain and relevant variables are indicated.

4. Results and discussion

4.1. The justification of the approaches

First, we will show that the parameter z_0 correlates with λ through the integration of Re $V(z)$ (equation (2)) being equal to a constant that determines the phase change of the electron waves. Hence it is essential and realistic to define equation (8) to reduce the infinity in solutions, as shown below.

The calculations were performed conventionally, as illustrated in [6], in which all the parameters are independent. Figure 4(a) shows an example of the correlation between z_0 and λ at 9.3 eV. There are three groups of correlation curves. The infinite couples of (z_{0i}, λ_i) along each of the three curves in a group provide matching between calculated and measured intensities $I_c/I_m = 1.00 \pm 0.05$, as indicated. The couples (z_{0i}, λ_i) ($i = 30$ sufficed for adequate statistics) on the central curve (labelled 1) in the upper two groups give the integrations of Re $V(z)$, from the second layer to infinitely large negative z, for values $I = 8.58 \pm 0.01$ and $I = 7.60 \pm 0.02$, as indicated in the diagram. It can be seen from the z_0–λ contour plot that λ decreases with increasing $-z_0$. If we define a function of $\lambda(z_0)$ which is orthogonal to the three z_0–λ curves (labelled 1), the three groups of infinite solutions will then be reduced to three finite ones. If we go further by treating all the SPB variables as functions of z_0, like in equations (7.2) and (7.3), uniqueness will be realized. Hence, it is justified to limit all the SPB parameters to being functions of one variable, namely the characteristic position of the electron distribution, $z_0(E)$.

We now show that uniqueness of solutions is realized by the single-variable parameterization of the non-uniform-SPB approach. Figures 4(b) and (c) show the z_0-

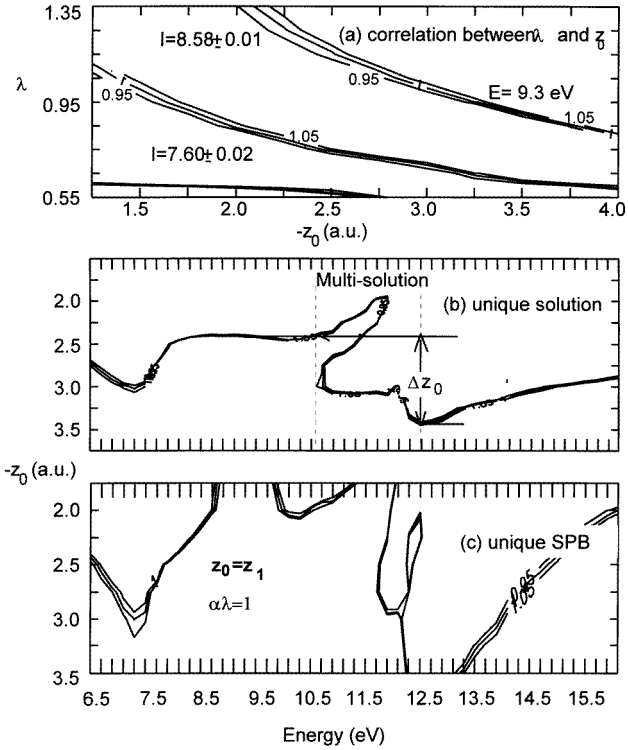

Figure 4. In (a) it is shown that λ is correlated with z_0 through the integration of Re $V(z)$ being equal to a constant, indicated for each curve, which provides the experimental foundations of the single-variable parameterization of the SPB (equation (8)). In (b) and (c) are shown the z_0–E profiles replicating the spectrum at 43.5° azimuth. Plot (b) is the standard case of equations (7.2) and (7.3) whereas (c) is modified to $z_1 = z_0$ and $\alpha = 1/\lambda$.

scanning solutions for various SPB approximations. The $z_0(E)$ curves provide matching of the calculated with the measured VLEED spectrum at 43.5°. Figure 4(b) is the ideal case (equations (7.2)–(7.3)) whereas figure 4(c) is modified with $z_1 = z_0$ and $\alpha\lambda = 1$. This modification means that the spatial decay Im $V(z)$ is identical to the Fermi part of Re $V(z)$. Except for the region 10.5–12.5 eV, a unique solution is obtained in figure 4(b). Obviously, figure 4(c) is excluded from consideration owing to the steeply varying dips with too large a Δz_0. Evidently, the model assumptions expressed by equations (6)–(8) are substantially correct.

4.2. The geometrical dependence of the $z_0(E)$ profiles

VLEED I–V curves are determined by the crystal geometry, and the electron distribution in the energy [Im $V(E)$] and real [Re $V(z)$, Im $V(z)$] spaces. It was demonstrated in [4] that the parameters in Im $V(z)$ determine the absolute intensity whereas the parameters in Re $V(z)$ dominate the shape of the spectra. Ideally, $z_0(x, y)$ represents the contour of the surface electron density detected with STM. In reality, as pointed out by Lindroos *et al* [10], the SPB parameters are functions of the energy E, the lateral component of the wavevector $k_\parallel$ and surface coordinates but the resultant $z_0(E, k_\parallel(x, y))$ is so complicated

that it is impractical in a modelling approach to separate the real-space and reciprocal-space contributions to the spectral intensity. Because VLEED integrates over a large surface area $z_0(E)$ exhibits joint features of topography and spectroscopy. Multiple and high-order diffractions merely provide minor modifications of the general shape of the $z_0(E)$ profile because these diffractions are very insignificant at very low energies [6, 10].

We now compare the z_0-optimizing results of the VLEED spectrum at 43.5° azimuth using the atomic positions given in figure 3 and table 1. Figure 5 shows the overlap matching between the calculated and the measured (00) beam reflectivity (I_{00}/I_0) as well as the corresponding $z_0(E)$ profiles. It is worthy of mention that the multi-solution for the range 10.5–12.5 eV that appeared on the z_0–E plot in figure 4(b) is automatically refined by the z_0-optimizing method, as can be seen by comparing figure 4(b) with profile A in figure 5(b). From figure 5(a) it can be seen that the agreement of the spectrum at 43.5° azimuth is *ultimately* realized by using the non-uniform SPB instead of the conventional uniform SPB [6]. Our aim in this work has been attained insofar as all the considered crystal structures provide a spectral match, but the corresponding $z_0(E)$ curves are different. That the minor difference in atomic positions results in an observable variation in the $z_0(E)$ profile is further evidence that the VLEED is considerably sensitive to the crystal geometry [3–6, 10]. The geometrical dependence of the $z_0(E)$ curve allows us to judge a model by simply comparing the shape of the $z_0(E)$ profile with those of others.

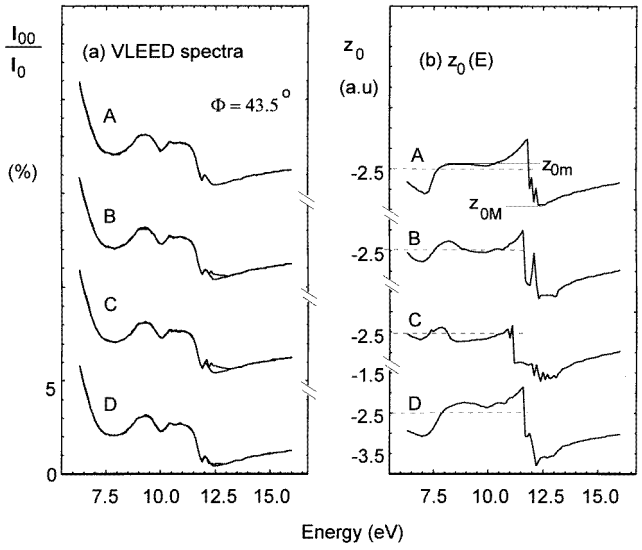

Figure 5. A matching fit of the spectrum (a) with the compared atomic positions in the Cu(001)-($\sqrt{2}\times 2\sqrt{}$)R45°-O structure given in table 1 and the corresponding variations in $z_0(E)$ (b). That which is being pursued in the current modelling is the claim that all the structures can be fitted yet yielding different $z_0(E)$ profiles. The structure can be judged by analysing the crystal-dependent $z_0(E)$ curves that exhibit joint features of topography and spectroscopy as revealed with STM/S and, besides, in terms of the physical interpretations provided by the model.

We may assign the atomic position (table 1) in the Cu(001)-($\sqrt{2}\times 2\sqrt{2}$)R45°-O structure as being the one approaching the true situation by carefully analysing the shape of the $z_0(E)$ curve against the criteria established. From the perspective of energy, features on the $z_0(E)$ curves below 7.5 eV coincide with the STS profiles [13] showing the occupied DOS

below E_f on the Cu(110)–O surface, which has been attributed to sp^3-type hybridization of oxygen [3–5]. The sharp features in the range 11.5–12.5 eV correspond to the reflection of the band gap at the boundary between Brillouin zones [1, 4, 10, 34, 35]. Consequently, the surrounding features relate to electron excitation at the edges of different energy bands. Curves B and C present extra features around 8.0 eV relative to those in A and D. From the spatial point of view, the difference between z_{0m} and z_{0M} varies considerably with the crystal structure, as given in table 1. We found that structure A provided the smallest Δz_0 and was closer to the STM scale difference of 0.45 Å [12], even though the former had been convoluted by the high-order diffraction and the latter by the tip size. Thus, the calculations favour the atomic positions assigned in A. Therefore, VLEED optimization outcomes support the conclusion about the O–Cu(001) reconstruction drawn by Nørskov *et al* [16, 20], namely that the O atoms go underneath the first layer for bonding. At the same time there is a pairing of Cu atoms/dipoles over the missing row. In fact, as described in equation (9), the paring dipoles and the missing-row vacancies originate from the Cu_3O_2 surface bonding [3–5].

4.3. The behaviour of surface electrons

The underlying physics of the above results agrees with the modelling assumptions. With these results we may deepen our insight into the behaviour of surface electrons and quantify the localized features observed with STM [12–16, 19]. In the dipole region, $z_1 \cong z_0$ and $\alpha \leqslant \lambda^{-1}$. This means that the metal dipoles enhance the SPB through the outwards shift of the wavefunction, giving a high degree of saturation. For the O–Cu(001) surface example (equation (8) and column A in table 1), z_{0M} is $(z_{0M}/z_0(\mathrm{Cu}) = 3.37/2.50)$ 1.35 times that of pure Cu(001) and λ_M is $(\lambda_M/\lambda(\mathrm{Cu}) = 1.27/0.9)$ about $\sqrt{2}$ times that of pure Cu(001) [7]. The conduction electrons colonize the structure and form electron islands, as observed in [12]. The values of z_{0M} and λ_M quantify the protrusions in the STM image in that the greater the protrusion, the greater the electron density. In the missing-row site, $z_1 \ll z_0$ and $\alpha \gg \lambda^{-1}$, that is, the missing-row vacancy is not occupied by 'free electrons', leading to the depression in the STM image. On the O–Cu(001) surface, the lowest degree of saturation of the SPB is $(\lambda_m/\lambda(\mathrm{Cu}) = 0.65/0.9)$ about $1/\sqrt{2}$ times that of Cu(001). Therefore, the electrons of the surfaces with chemisorbed oxygen are rather localized. We may describe the O–metal surface as a non-Fermi system without freely moving electrons. Knowledge of this mechanism may improve our understanding of the metal oxides with lower work functions but higher contact electric resistivities.

The O-induced non-uniformity in the electric potential/field should have an influence on further reaction of a surface, as observed by Kostov *et al* [36] in the synthesis of isocyanate (NCO) on Ru(001). It was found by Kostov *et al* that the isocyanate could be formed only in the presence of pre-adsorbed oxygen atoms. They suggested two possible mechanisms for the effect of pre-adsorbed on the reaction. One is the influence of the strong dipole field; the other is the strong site specificity of the O adsorbate which forces either one or both reactants (C, N) onto different, more reactive, sites compared with those for the situation without O. According to the current modelling computations, the gradient of $\mathrm{Re}\,V(z)$ is also site-dependent. The electric field is much stronger at dipole sites than is that of clean surfaces and that of STM depressions for systems with chemisorbed oxygen. Fujita *et al* [19] observed the site specificity of the oxygen atoms, which are adsorbed on the next-nearest-neighbour sites of Cu(001). Both the current modelling formulation and Fujitas' recent STM observation support the proposals of Kostov *et al*. From the viewpoint of surface bonding, we may further suggest that the ionization and polarization of surface

atoms by the highly electronegative O adsorbate may provide electron accepter/donor sites for further bonding to form the isocyanate (the electronegativities of C, N and O are 2.5, 3.0 and 3.5, respectively [30]). Hence, it should be true that the effects of the dipole moment and site specificity are intimately intertwined, as discussed by Kostov *et al* [36].

5. Conclusion

It has been demonstrated that the current modelling of the *single-variable parameterized non-uniform SPB* is able to illustrate the behaviour of electrons on metal surfaces with chemisorbed oxygen. The formulations can reasonably well quantify the localized features revealed by STM and STS. As an important factor determining the interaction between incident electrons and the surface, the variation of the energy state can be obtained from the $z_0(E)$ profile. Because the $z_0(E)$ profiles vary with crystal structure, the difficulty of simultaneously identifying the crystal structure and the electronic distribution has thus been overcome completely with simplified optimizations. The combination of VLEED and STM/S furnished with appropriate modelling approximations is much more efficient than either of them alone in providing quantitative information not only about the bonding dynamics [5] but also for crystallography, microscopy and spectroscopy. The consistency among the VLEED profiles $z_0(E)$, STM and STS observations is evidence that our single-variable parameterized non-uniform SPB is essentially appropriate, as has been demonstrated in recent works [4, 5].

Acknowledgments

Beneficial discussions with P Jennings and critical review by A Stelbovics, P Jennings, S Tear, M Donath and G Russell as well as the kind provision of VLEED data by G Hitchen and also of the original code by S Thurgate are all gratefully acknowledged.

References

[1] Jones R O and Jennings P J 1988 *Surf. Sci. Rep.* **9** 165
[2] Pendry J B 1974 *Low Energy Electron Diffraction: The Theory and its Application to the Determination of Surface Structure* (London: Academic)
[3] Sun C Q and Bai C 1997 A model of bonding between oxygen and metal surfaces *J. Phys. Chem. Solids* **58** 903–12
[4] Sun C Q 1997 Spectral sensitivity of the VLEED to the bonding geometry and potential barrier of the O–Cu(001) surface *Vacuum* **48** 481–8
[5] Sun C Q 1997 Exposure-resolved VLEED from the O–Cu(001): bonding dynamics *Vacuum* **48** at press
[6] Thurgate S M and Sun C Q 1995 *Phys. Rev.* B **51** 2410
[7] Dietz R E, McRae E G and Campbell R L 1980 *Phys. Rev. Lett.* **45** 1280
[8] Hitchen G, Thurgate S M and Jennings P J 1991 *Phys. Rev.* B **44** 3939
[9] Jones R O, Jennings P J and Jepsen O 1984 *Phys. Rev.* B **29** 6474
[10] Lindroos T, Pfnür H and Menzel D 1986 *Phys. Rev.* B **33** 6684
Pfnür H, Lindroos M and Menzel D 1991 *Surf. Sci.* **248** 1
[11] McRae E G and Caldwell C W 1976 *Surf. Sci.* **57** 766
[12] Jensen F, Besenbacher F, Lagsgaard E and Stensgaard I 1990 *Phys. Rev.* B **41** 10 233
[13] Chua F M, Kuk Y and Silverman P J 1989 *Phys. Rev. Lett.* **63** 386
Kuk Y, Chua F M, Silverman P J and Meyer J A 1990 *Phys. Rev.* B **41** 12 393
[14] Koch R, Schwarz K, Schmidt K, Burg B, Christmann K and Rieder K H 1993 *Phys. Rev. Lett.* **71** 1047
[15] Wintterlin J and Behm R J 1992 In *Scanning Tunnelling Microscopy I* (Berlin: Springer) ch 4
[16] Besenbacher F and Nørskov J K 1993 *Prog. Surf. Sci* **44** 5

[17] Lang N 1983 *Surf. Sci.* 127, L118
Lang N 1989 *Comm. Cond. Matt. Phys.* **14** 253
[18] Ertl G and Rhodin T N 1979 *The Nature of the Surface Chemical Bond* (Amsterdam: North-Holland)
[19] Fujita T, Okawa Y, Matsumoto Y and Tanaka K 1996 *Phys. Rev.* B **54** 2167
[20] Jacobsen K W and Nørskov J K 1990 *Phys. Rev. Lett.* **65** 1788
[21] Rotermund H H 1993 *Surf. Sci.* **283** 87
Rotermund H H, Lauterbach J and Hass G 1993 *Appl. Phys.* A **57** 507
Lauterbach J, Asakura K and Rotermund H H 1994 *Surf. Sci.* **311** 322
[22] Lederer T, Arvanitis D, Comelli G, Troger L and Baberschke K 1993 *Phys. Rev.* B **48** 15 390
[23] Zeng H C and Mitchell K A R 1990 *Surf. Sci.* **239** L571
[24] Jennings P J private communication
[25] Beiser A 1988 *Perspectives of Modern Physics* 18th edn (Singapore: McGraw-Hill)
[26] Ertl G 1994 *Surf. Sci.* **299/300** 742
[27] Hitchen G, Thurgate S M and Jennings P J 1988 *Phys. Rev.* B **38** 8668
[28] Van Hove M A and Tong S Y 1979 *Surface Crystallography by LEED* (Berlin: Springer)
[29] Atrei A, Bardi U, Rovida G and Zanazzi E 1990 *Vacuum* **41** 333
[30] Keenan K W, Kleinfelter D C and Wood J H 1979 *General College Chemistry* 6th edn (New York: Harper & Row)
[31] Pauling L 1960 *The Nature of the Chemical Bond* 3rd edn (New York: Cornell University Press)
[32] Goldschmidt V M 1927 *Ber. Deutsch Chem. Ges.* **60** 1270
[33] Cole A P, Root D E, Mukherjee P, Soloman E I and Stack T D P 1996 *Science* **273** 1848
[34] Strocov V N 1991 *Solid State Commun.* **78** 545
Strovoc V N 1993 *Int. J. Mod. Phys.* B **7** 2831
Strocov V N 1995 *Int. J. Mod. Phys.* B **9** 1755
[35] Bartos I and Koukal J 1991 *Surf. Sci.* **251/252** 508
[36] Kostov K L, Rausche H and Menzel D 1993 *Surf. Sci.* **287/288** 283